Surface & Coatings Technology 205 (2011) 2857–2864

Contents lists available at ScienceDirect

Surface & Coatings Technology

journal homepage: www.elsevier.com/locate/surfcoat

Corrosion protection by multilayer coating using layer-by-layer technique

E.C. Gomes *, M.A.S. Oliveira

Instituto Tecnológico de Aeronáutica (ITA), Chemistry Department and Aeronautics-Mechanics Division, Gas Turbine Reference Center, Pça, Mal Eduardo Gomes, 50 CTA, São José dos Campos, SP, CEP 12 228-900, Brazil

ARTICLE INFO

Article history:
Received 11 January 2010
Accepted in revised form 26 October 2010
Available online 1 November 2010

Keywords:
Polyaniline
PVSS
Layer-by-layer
EIS
2024 alloy
Corrosion

ABSTRACT

In this work, polyaniline (PAni), a polycation, and poly (vinylsulfonic acid, sodium salt) (PVSS), a polyanion, were used for preparing multilayer thin films on AA2024 alloy surface using the layer-by-layer growth technique. The corrosion of AA2024 alloy surfaces coated with a number n (n = 0, 1, 5, 8, 10, 15) of multilayered thin films was investigated in 0.1 M NaCl aqueous solutions using potentiodynamic polarization, chronoamperometry and electrochemical impedance spectroscopy (EIS) techniques. These electrochemical tests were conducted at a temperature of (25 ± 2) °C. Surface coated with 08 (PVSS / PAni) bilayers presented greater resistance to corrosion in the chloride containing environment.

1. Introduction

Surface treatment of metals using chromium compounds is becoming economically unfeasible due to various environmental constraints. Material treated by this type of process, has faced problems of rejection in the market. To be feasible, the development of new chromium free technologies should lead to a similar or improved corrosion resistance compared to current processes and equivalent process cost to those ones of chromium (VI) based products. One of the new technologies for the replacement of chromium is the use of multilayer thin films produced by layer-by-layer growth technique.

Coating of metallic surfaces with conductive polymers has been used to protect oxidizable metals, such as carbon steel [1–5], aluminum [6,7] and stainless steel [8,9], against corrosion. The advantage of these coatings over others, such as paints, is that they do not contain toxic substances that are harmful to the environment, and their production process is simple and economical [10]. Furthermore, as these polymers can carry specific molecular groups on their structures, or can be doped with specific anions, they may shift the coated material potential to values at which the corrosion rate of the underlying metal is significantly reduced [10].

Polyaniline (PAni) is a polymer that can present a conductive form. Depending on the level of protonation and oxidation, PAni exists in various forms with different physical properties [11,12]. For instance, in the emeraldine base form, PAni is a dielectric material having conductivity in the range of 10^{-11} to 10^{-8} Scm^{-1}. In a protonated form (emeraldine salt) the polymer has conductivity in the order of 10^{1} Scm^{-1} [13]. Due to its facility of chemical and electrochemical synthesis, thermal stability in air, redox behavior, low cost, versatile processability, electrical conductivity and relative stability, polyaniline (PAni) has attracted a particular interest in technological applications such as batteries [14], sensors [15], electrochromic devices, capacitors [16], solar cells, blends and resistant to corrosion coatings.

Protonated polyaniline can be chemically obtained by oxidation of aniline in acid media [11,17]. It can be readily converted to its corresponding base form by treating the conductive PAni emeraldine salt form with an alkaline solution, such as ammonium hydroxide solution [18].

Since highly conductive forms of many conductive polymers frequently present low solubility, and are infusible, the ability of processing electrically conductive polymers into thin films, controlling film thickness and creating uniform pinhole-free films is oftentimes extremely challenging and important [19,20].

Partially doped polyaniline is readily and spontaneously adsorbed on many different types of substrate surfaces, including both hydrophilic and hydrophobic, such as platinum-coated glass, gold-coated glass, aluminum-coated glass, mica, graphite, silicon, and polymers [19]. This fact has been used to fabricate multilayer thin films of polyaniline in a layer-by-layer approach. In one of the layer-by-layer multilayer film growth procedures, a monolayer of a polyanion is first adsorbed on a surface, followed by rinsing, to remove excesses of the non-adsorbed material, and subsequent dipping into a dilute aqueous solution of a polycation, aqueous solution of a protonated polyaniline for instance. The adsorption of positively charged polyaniline onto the negatively charged surface changes the net surface charge from negative to positive, thereby

* Corresponding author. Tel.: +55 12 3947 6953.
E-mail address: evertonquimica@gmail.com (E.C. Gomes).

0257-8972/$ – see front matter.
doi:10.1016/j.surfcoat.2010.10.061

making it possible to adsorb another layer of negatively charged polyanion. This process can be repeated as many times as desired to create multilayer thin films consisting of semi-interpenetrated polyanion/polyaniline alternating layers (the level of layer interpenetration depends on many factors including solution concentration and surface charge density) [20]. In this case, the cationic nature of partially doped polyaniline promotes a multilayer assembly via electrostatic attractions with the polyanion.

The building of a multilayer film on AA2024 alloy surfaces prior to painting must improve the painting film adhesion by forming a compact and homogeneous layer with good stability on the metal / multilayer film interface.

In this work, polyaniline (PAni), a polycation, and Poly (vinylsulfonic acid, sodium salt) (PVSS), a polyanion were used to form multilayer films on AA2024 alloy surfaces. The polyaniline (PAni) was chemically synthesized [21,22]. The corrosion inhibition afforded by the deposited films using the layer-by-layer growth technique was investigated in 0.1 M NaCl aqueous solutions by electrochemical impedance spectroscopy (EIS), potentiodynamic polarization and chronoamperometric techniques.

2. Materials and methods

The PAni was chemically synthesized [21,22] using the monomer, previously distilled under vacuum, and an oxidant (monomer/oxidant molar ratio of 4:1). The synthesis was performed in aqueous solution of HCl (1 mol L^{-1}) in temperatures between 0 and 2 °C. Under these conditions, the polymer is obtained in its doped form PAni-HCl [23], slightly soluble in water. In order to increase the solubility of the obtained polyaniline in aqueous medium, the PAni-HCl was subjected to a process of de-doping using a 1 mol L^{-1} ammonium hydroxide solution, obtaining the de-doped PAni (PAni-NH_4OH), and re-doping using a solution of concentrated formic acid, obtaining the re-doped polymer PAni-HCOOH, soluble in concentrated formic acid aqueous solutions [24]. The PAni-HCOOH was used in the production of self-assembled films on the surface of the AA2024 alloy.

Disc-shaped bodies of the AA2024 alloy, measuring 36 mm in diameter and 2 mm thick, were grounded using, in the sequence, 120, 220, 320, 400, 600 and 1200 SiC paper, polished with aqueous slurry of 3 μm alumina, and degreased with methanol, under ultrasound, for about 15 minutes.

The poly (acid vinylsulfonic salt sodium) (PVSS) (Sigma-Aldrich) was used as an aqueous solution with a concentration of 1.2 g L^{-1}.

The deposition of the films was done, primarily, by immersion of the metallic substrate in the poly (acid vinylsulfonic salt sodium) (PVSS) solution. After 5 min of immersion, the substrate was withdrawn from the polyanion solution and dried in a hot air stream. Then the substrate was immersed in an aqueous solution of the PAni dissolved in concentrated formic acid (about 2% w/w of PAni-HCOOH) and after 5 minutes of immersion in this solution, it was washed with demineralized water and then dried in hot air stream. The repetition of the two processes (immersion in the solution of polyanion followed by immersion in the solution of the polycation) led to the formation of the (PVSS / PAni) multilayer films.

Potentiodynamic polarization, chronoamperometric and electrochemical impedance spectroscopy (EIS) tests were performed for both, polished and multilayer films covered surfaces. In these tests, an Autolab Potentiostat/Galvanostat, with a Frequency Analyzer, Model PGSTAT30, controlled by the GPES and the FRA.EXE software, both of them, respectively installed in a micro computer interfaced to the potentiostat through the USB-IF030 interface, were used. The electrochemical cell was a cell with three electrodes configuration: working, reference and counter-electrode. The reference electrode in all experiments was a (Ag / AgCl, Cl^-) saturated electrode, the counter-electrode was a spiral platinum wire and the working electrode was the AA2024 alloy surface, polished and coated with the multilayer films. The exposed area of the working electrodes was 0.502 cm^2. The electrolyte solution used in all electrochemical experiments was a NaCl (VETEC) aqueous solution. The NaCl concentration in this solution was 0.1 mol L^{-1}. All tests were performed in triplicate, at temperature of (25 ± 2) °C.

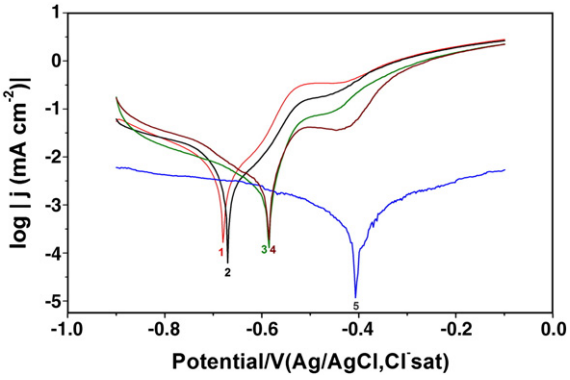

Fig. 1. Potentiodynamic polarization curves, in 0.1 mol L^{-1} NaCl aqueous solution, for AA2024 alloy surface coated with a number n of (PVSS / PAni) bilayers deposited using the layer-by-layer growth technique. (1) n = zero (polished surface), (2) n = 1, (3) n = 5, (4) n = 10 and (5) n = 8. Potential scan rate of 5 mV s^{-1}.

In the potentiodynamic polarization experiments, the potential was varied from a value 400 mV lower than the open circuit potential up to 400 mV higher than this potential. The potential scan rate was 5 mV s^{-1}. The chronoamperometric experiments were performed over a range of 3600 seconds applying a potential 100 mV more positive than the corrosion potential (Ecorr). The impedance spectra were obtained in the frequency range of 10 kHz to 0.01 Hz. A sinusoidal AC voltage excitation of 5 mV, superposed to the stationary open circuit potential, was used in the EIS studies. The software EQUIVCRT, developed by the Boukamp group [25], was used to determine the parameters related to the electrical equivalent circuits used to describe the electrochemical process occurring on each surface exposed to the aqueous solution containing chloride.

The morphology of the (PVSS / PAni) multilayer coated surfaces was investigated using scanning electron microscopy (SEM) (Jeol JXA-840A). The energy of the SEMs electron beam was 15 kV.

3. Results and discussion

Fig. 1 shows the anodic polarization curves for the AA2024 alloy covered with different numbers of (PVSS / PAni) multilayers. The corrosion potential (Ecorr) and corrosion current densities (Jcorr) obtained from these curves are presented in Table 1.

Independent on the number of bilayers, the corrosion potential (Ecorr) of the aluminum alloy coated surfaces shifted to less negative values. This displacement is bigger for the surface coated with a number of 08 bilayers, indicating that this surface has a smaller

Table 1
Corrosion parameters of the AA2024 alloy surfaces coated with a number n (n = 0, 1, 5, 8 and 10) of (PVSS / PAni) bilayers deposited layer-by-layer, exposed to an aqueous solution of NaCl at the temperature of (25 ± 2) °C.

Surface	Ecorr (V/Ag/AgCl, Cl^-)	Jcorr (mA cm^{-2})	Rp (Ω cm^2)
Aluminum AA2024	−0.67 ± 0.05	(10 ± 3) × 10^{-3}	(1.06 ± 0.04) × 10^4
1 bilayer (PVSS / PAni)	−0.66 ± 0.05	(10.3 ± 0.6) × 10^{-3}	(1.20 ± 0.5) × 10^4
5 bilayers (PVSS / PAni)	−0.58 ± 0.007	(3.5 ± 1) × 10^{-3}	(4.20 ± 0.5) × 10^4
8 bilayers (PVSS / PAni)	−0.43 ± 0.007	(7.0 ± 0.7) × 10^{-4}	(1.43 ± 0.06) × 10^5
10 bilayers (PVSS / PAni)	−0.59 ± 0.06	(3.0 ± 1) × 10^{-3}	(1.00 ± 0.5) × 10^4

Table 2
Inhibiting efficiency (η) of the multilayer films formed on the AA2024 alloy surfaces exposed to 0.1 mol L^{-1} NaCl aqueous solution.

Number of multilayers	Inhibiting efficiency (η) %
1 bilayer	3.0
5 bilayers	65.0
8 bilayers	93.0
10 bilayers	70.0

Table 3
Inhibiting efficiency (η) of the multilayer films formed on the AA2024 alloy surfaces exposed to 0.1 mol L^{-1} NaCl aqueous solution.

Number of multilayers	Inhibiting efficiency (η) %
1 bilayer	6.0
5 bilayers	15.0
8 bilayers	70.0
10 bilayers	47.0

tendency to corrode. The corrosion current density (Jcorr), obtained by the extrapolation of the anodic and cathodic branches of the Tafel curves [26], is also lower for the surface coated with 08 bilayers of (PVSS / PAni). Therefore, 08 is the number of bilayers offering better corrosion protection to the AA2024 alloy surface in the environment containing chloride.

From the results shown in Table 1, the inhibiting efficiency (η) of the films covering the AA2024 alloy surface was calculated using Eq. (1) [27]:

$$\eta = \frac{(J_{without/film} - J_{with/film})}{J_{without/film}} \times 100 \quad (1)$$

where J is the electric current density values presented in Table 1. The results of this calculation are showed in Table 2.

Fig. 2 shows the chronoamperometric curves for the AA2024 alloy coated with different n numbers of (PVSS / PAni) bilayers.

The chronoamperometric results show a decrease in the current density (J) of the AA2014 alloy coated surfaces exposed to the NaCl aqueous solution. This decrease in the electric current density is bigger for surfaces coated with 08 bilayers. This observation, once more, demonstrates that the best corrosion protection is provided by the 08 (PVSS / PAni) bilayer films.

From the results shown in Fig. 2, the inhibiting efficiency (η) of the films covering the AA2024 alloy surface was calculated using Eq. (1) [27], where J is the electric current density values at the fixed time of 3000 seconds. The results of this calculation are shown on Table 3.

The inhibiting efficiency (η) obtained from the chronoamperometric results (Table 3) is lower than those obtained from the potentiodynamic polarization results (Table 2). As the overpotential to which the surfaces were submitted during the chronoamperometric experiments was lower than those experienced by those surfaces submitted to the potenciodynamic experiments, a new phase formation, due to an electrooxidation process, should have contributed to an increase of the surfaces resistance during the potentiodynamic polarization experi-

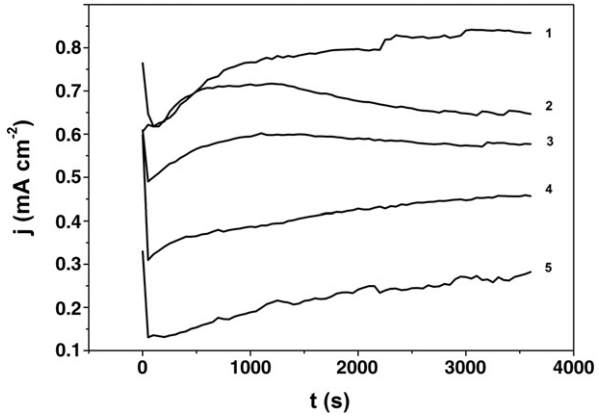

Fig. 2. Chronoamperometric curves, in 0.1 mol L^{-1} NaCl aqueous solution, for AA2024 alloy surface coated with a number n of (PVSS / PAni) bilayers, where (1) n = zero (polished surface), (2) n = 1, (3) n = 5, (4) n = 10 e (5) n = 8. A +100 mV potential was applied to the corrosion potential (Ecorr).

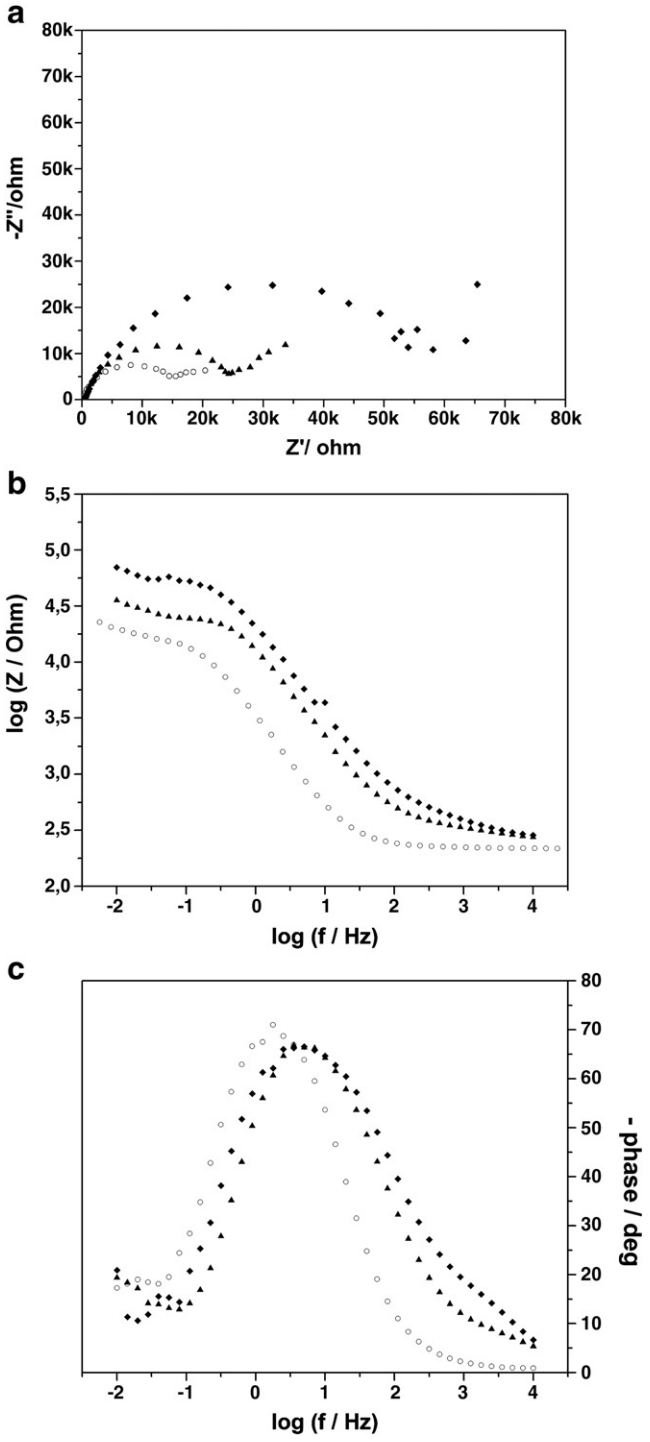

Fig. 3. Diagrams of: (a) Nyquist, (b) and (c) Bode plots of AA2024 alloy surfaces covered with, respectively, 0 (○) , 08 (♦) and 10 (▲) (PVSS / PAni) bilayer films, in 0.1 mol L^{-1} NaCl aqueous solution.

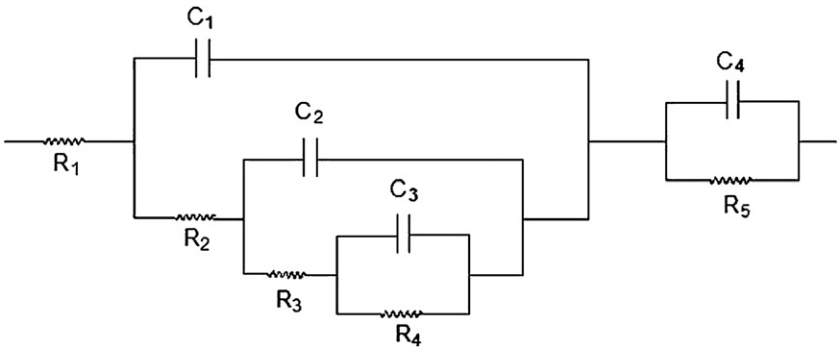

Fig. 4. Equivalent electric circuit model used to simulate the EIS results of the AA2024 aluminum alloy exposed to a 0.1 mol L^{-1} NaCl aqueous solution.

ments. However, as the chromoamperometric as the potentiodynamic results presented the same trend.

Fig. 3 shows representative Nyquist diagrams (a) and Bode plots (b and c) for the AA2024 alloy surface, coated with 0, 08 and 10 (PVSS / PAni) bilayer films, exposed to a 0.1 mol L^{-1} NaCl aqueous solution. In the Nyquist Plot, the imaginary component (Z″) is plotted against the real (Z′) component of the impedance, while in the Bode Plot, the logarithm of the absolute value of impedance (Z) and phase angle (ϕ) are plotted against the logarithm of frequency (f) of the AC potential applied to the electrochemical cell.

The Nyquist diagrams presented in Fig. 3(a) may be approximated to a semicircle in regions of high frequency. The intercepts of this semicircle with the X axis, i.e. the diameter of the semicircle, are related to the resistance of the film. In the Nyquist diagrams of the aluminum alloy surfaces coated with films deposited by layer-by-layer growth technique the diameter of this semicircle is larger than that one in the Nyquist diagram of the alloy without any film. This observation allows us to suggest that surfaces of the alloy AA2024 coated with the layer-by-layer grown films show greater resistance to oxidation than the ones of the uncoated alloy.

The presentation of the impedance data as a Bode plot gives information that helps to ascertain more directly the different constituent phases of the system. Thus, in those frequency regions where a resistive behavior is dominant, a horizontal line is observed for the log Z vs log f representation and a ϕ close to 0° is measured. Also, in the log Z vs log f plots, a capacitive behavior within a frequency region is described by a straight line with a slope of −1 and a ϕ around 90°, whereas the diffusion-controlled phenomena (Warburg impedance) would give a straight line with a slope of −1/2 and a ϕ of 45°. In the Bode plots presented in Fig. 4(b) it is observed that, independent on the frequency, the impedance of surfaces of the AA2024 alloy coated with (PVSS / PAni) bilayers is greater than that one of the uncoated alloy. This observation reinforces the conclusion that, in a medium containing chloride, the resistance to corrosion of the AA2024 alloy surfaces coated with (PVSS / PAni) bilayer films is greater than that one of the polished alloy surface.

In addition to the time constants observed at intermediate (~10^3–10^{-1} Hz) and low frequencies (~10^{-1}–10^{-2} Hz) in the angle phase diagram of the aluminum surface uncovered with multilayer films (Fig. 3c), the Bode angle phase diagram of the AA2024 alloy surface covered with 08 (PVSS / PAni) bilayers film revealed an additional time constant at frequencies between 10^4 and 10^3 Hz. This new time constant can be associated with the capacitance and resistance of the multilayer film covering the aluminum alloy surface. The Bode diagram of the surface coated with 10 (PVSS / PAni) bilayer film, also presents this third time constant.

Aluminum and its alloys exposed to air suffer oxidation and a double layer aluminum oxide film, which is composed by a compact internal and an open texture external oxide layer, are formed on their surface. This oxide film is subjected to hydration when exposed to air at relatively low temperatures (≈40 °C). The hydration process contributes to increase the film volume and diminishes the amount of defects present in the oxide film [28]. Considering this oxide structure, an equivalent electric circuit represented by $R_1(C_1[R_2(C_2[R_3(C_3R_4)])])(C_4R_5)$ in Boukamp's notation [29], shown in Fig. 4, was proposed to fit the EIS results obtained for the just polished aluminum alloy surface studied in this work.

According to the model shown in Fig. 4, the oxide film covering the AA2024 aluminum alloy is characterized by a low-frequency (LF) RC circuit consisted by a double layer capacitance (C_3) in parallel with a charge transfer resistance reaction ($R_4 = R_{ct}$); an intermediate-frequency (IF) CR circuit consisted of a hydrated oxide capacitor (C_2) in parallel with a hydrated oxide resistance (R_3); a high / intermediate-frequency (HF/IF) network consisting of a pore wall capacitor (C_1), in parallel with an internal pore wall resistance (R_2); a high / intermediate-frequency

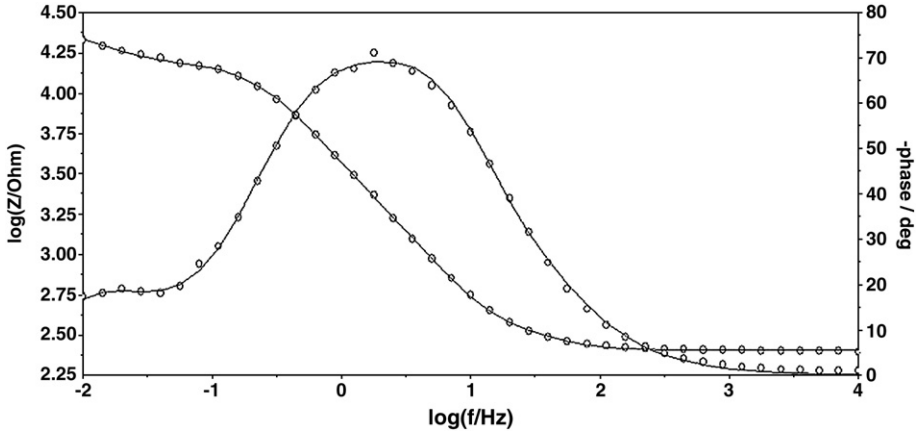

Fig. 5. Bode plot for uncoated AA 2024 alloy surface exposed to NaCl aqueous solution. An equivalent electrical circuit represented by $R_1(Q_1[R_2W_1])(Q_2[R_3(C_1[R_4W_2])])(C_2R_5)$, in Boukamp's notation [29] (full line), was used to simulate the experimental results.

Table 4
Electrochemical parameters obtained by simulation of the EIS results of the polished AA2024 alloy, exposed to a 0.1 mol L^{-1} NaCl aqueous solution, open to air, with a R_1 (Q_1 [R_2W_1]) (Q_2 [R_3 (C_1 [R_4W_2])]) (C_2R_5) equivalent electrical circuit model.

Parameter	Compact oxide layer (IF)/(HF)	Porous, hydrated oxide (IF)/(HF)	Interface porous oxide \/electrolyte (LF)
R_1 (Ω)		253	
C_1 (μF)	52.9		
R_2 (Ω)	107		
C_2 (μF)		101	
R_3 (kΩ)		0.59	
C_3 (mF)			1.22
$R_4 = R_{tc}$ (kΩ)			11.0
C_4 (μF)	48.8		
R_5 (kΩ)	14.0		

(HF/IF) CR circuit consisted of a barrier oxide capacitor (C_4) in parallel with a barrier oxide resistance (R_5).

Fig. 5 presents the experimental (empty circles) and the fitting simulation impedance results (full lines) obtained for the uncoated AA2024 aluminum alloy exposed to the 0.1 mol L^{-1} NaCl aqueous solution. The fitting simulation was performed with the equivalent electrical circuit model shown in Fig. 4.

A comparison between the experimental and the fitting results indicates that the proposed model is adequate to explain the behavior of the uncoated AA2024 alloy exposed to the NaCl aqueous solution. Table 4 shows the parameter values obtained by simulation using the proposed equivalent electric circuit model (Fig. 4).

The equivalent electric circuit shown in Fig. 6, represented by R_1 (C_1[R_2(C_2[R_3(Q_1[R_4W_1])])]) in Boukamp's notation [29], was proposed to fit the EIS results obtained for AA2024 alloy surface coated with 08 (PVSS / PAni) bilayer film.

The model illustrated in Fig. 6 considers that the 08 (PVSS / PAni) bilayer films formed on AA2024 alloy surface contain defects through which the electrolyte solution permeates favoring the corrosion process initiation. SEM micrographs, which will be presented late in this work, and show that the 08 layer-by-layer films formed on AA2024 alloy surface present pinholes and are very rough. In the model presented in Fig. 6, R_1 corresponds to an uncompensated resistance of the electrolyte solution, R_2 and C_1 represent, respectively, the capacitance (C_{Film}) and the resistance (R_{Film}) of the coat, R_3 and C_2 represent the capacitance and resistance of the porous oxide layer, Q_1 and R_4 represent the double layer constant phase element (CPE) (Q_{dl}) and resistance to charge transfer ($R_4 = R_{ct}$) of corrosion reactions, and W represents the resistance to diffusion of electroactive species in the respective phases. The impedance of the constant phase element (CPE) is defined by $Z_Q = [C(j\omega)^n]^{-1}$, where C is the capacitance of an ideal capacitor, $j = \sqrt{-1}$, ω is the angular frequency ($\omega = 2\pi f$) of the AC voltage applied to the electrolyte cell, and $0 < n < 1$ represents the deviation of the ideal capacitance behavior, which is related, for instance, to the surface roughness [30–32], porosity, etc. [33,34]. For $n = 1$, Z_Q represents the impedance of the ideal capacitor.

Fig. 7 shows the experimental (empty diamonds) and the fitting simulation of the impedance results (full lines) obtained for AA2024 alloy surface coated with 08 (PVSS / PAni) bilayer film and exposed to

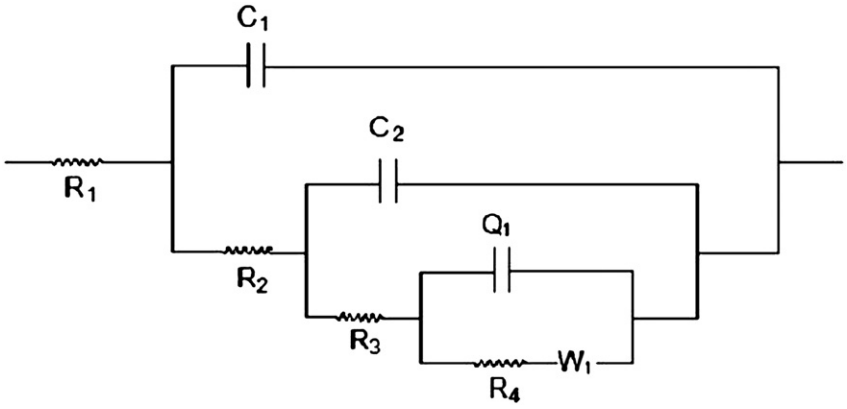

Fig. 6. Equivalent electric circuit model used to simulate the EIS results of the AA2024 aluminum alloy surface coated with film 08 (PVSS / PAni) bilayer film exposed to a 0.1 mol L^{-1} NaCl aqueous solution.

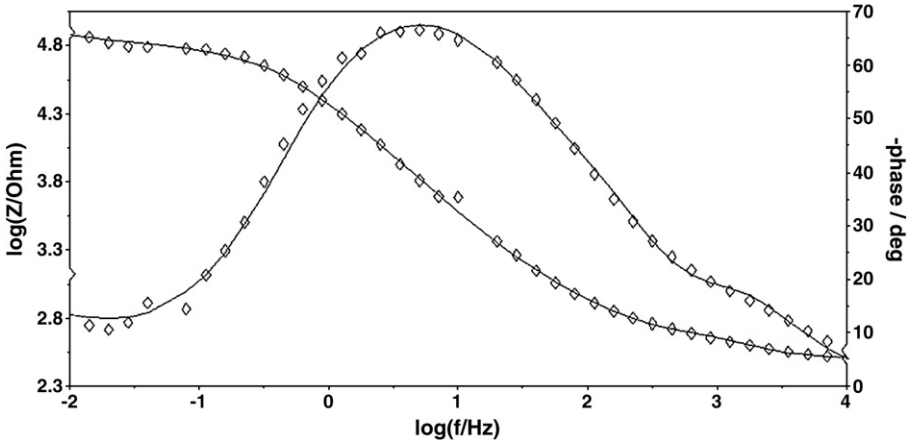

Fig. 7. Bode graph of AA2024 alloy surface coated with 08 (PVSS / PAni) bilayer film and exposed to a NaCl aqueous solution. An equivalent electrical circuit represented by R_1(C_1[R_2(C_2[R_3(Q_1[R_4W_1])])]), in Boukamp's notation [29] (full line), was used to simulate the experimental results.

Table 5
Electrochemical parameters obtained by simulation of the EIS results of AA2024 alloy surface coated with films 08 and 10 self-assembled bilayers, exposed to a 0.1 mol L^{-1} NaCl aqueous solution, open to air, with a $R_1(C_1[R_2(C_2[R_3(Q_1[R_4W_1])])])$ and $R_1(Q_1[R_2W_1])(Q_2[R_3(Q_3[R_4(Q_4[R_5W_2])])])$ equivalent electrical circuit, in Boukamp's notation [29].

Parameter	Film with 08 bilayers	Parameter	Film with 10 bilayers
R_1 (Ω)	285	R_1 (Ω)	279
C_1 (μF)	9.4	Q_1 (μF)	37.4
		n	0.62
R_2 (Ω)	244	R_2 (Ω)	22.8
C_2 (μF)	1.99	Q_2 (μF)	4.04
		n	0.89
R_3 (kΩ)	1.21	R_3 (Ω)	97.9
Q_1 (μF)	6.13	Q_3 (μF)	8.81
n	0.81	n	0.94
R_4 (kΩ) = R_{ct}	54.3	R_4 (kΩ)	6.45
		Q_4 (μF)	3.76
		n	0
		R_5 (kΩ) = R_{ct}	16.3

the 0.1 mol L^{-1} NaCl aqueous solution. The fitting simulation was performed with the equivalent electrical circuit model shown in Fig. 6.

A comparison between the experimental and simulated results indicates that the proposed model is adequate to explain the behavior of AA2024 alloy surface coated with 08 (PVSS / PAni) bilayer films and exposed to a NaCl aqueous solution. The values of the parameters obtained by simulation of the EIS data using the proposed equivalent electric circuit model (Fig. 6) are presented in Table 5.

The equivalent electric circuit shown in Fig. 8, represented by $R_1(Q_1[R_2W_1])(Q_2[R_3(Q_3[R_4(Q_4[R_5W_2])])])$ in Boukamp's notation [29], was proposed to fit the EIS results of AA2024 alloy surfaces coated with 10 (PVSS / PAni) bilayer films and exposed to 0.1 mol L^{-1} NaCl aqueous solution.

The model illustrated in Fig. 8 considers what is shown in the SEM micrographs of AA2024 alloy surfaces coated with 10 (PVSS / PAni) bilayer films, which will be presented later in this work, i.e., it considers that the 10 (PVSS / PAni) bilayer films are more homogeneous than the 08 (PVSS / PAni) bilayer films covering the aluminum alloy surface. But, despite this fact, the 10 bilayer films contain defects, inside which a thin film layer of the (PVSS / PAni) bilayer film covers the metallic substrate, and electrolyte solution permeates through this thin bilayer film layer, favoring the corrosion process.

In the model presented in Fig. 7, R_1 corresponds to an uncompensated resistance of the electrolyte solution, R_2 and Q_1 represent, respectively, the resistance (R_{Film}) and the CPE (Q_{Film}) associated with the capacitance of the coating, R_3 and Q_2 represent the resistance and CPE associated to the capacitance of the porous oxide layer, Q_3 and R_4 represent, respectively, the CPE constant phase element and resistance associated to pores in the oxide barrier in contact with the metallic substrate. Finally, Q_4 and R_5 represent the double layer constant phase element (CPE) and resistance to charge transfer ($R_5 = R_{ct}$) of corrosion reactions, and W represents the resistance to diffusion of electroactive species in the respective phases.

Fig. 9 shows the experimental (empty triangle) and the fitting simulation impedance results (full lines) obtained for AA2024 alloy

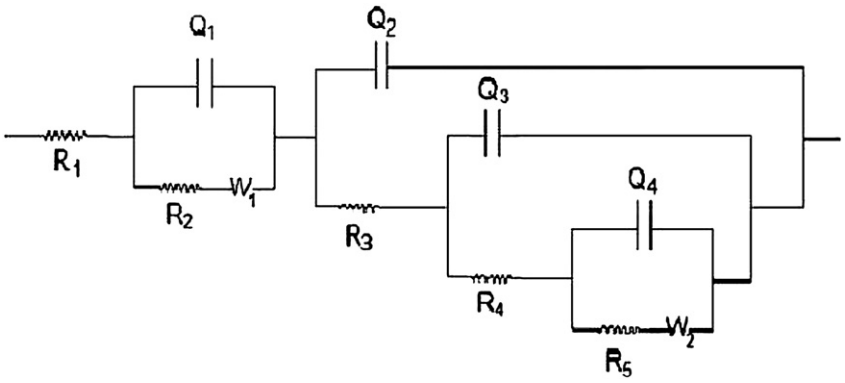

Fig. 8. Equivalent electric circuit model used to simulate the EIS results of the AA2024 alloy surface coated with 10 self-assembled (PVSS / PAni) bilayer films and exposed to a 0.1 mol L^{-1} NaCl aqueous solution.

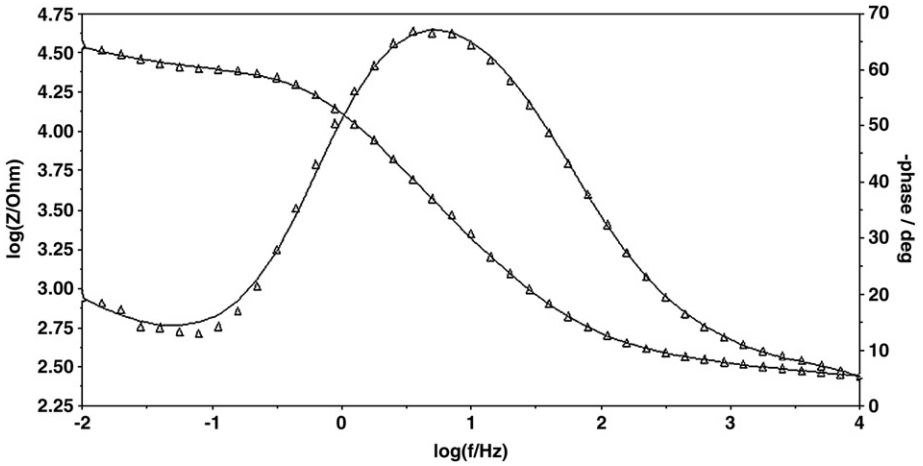

Fig. 9. Bode graph obtained for an aluminum surface coated with 10 (PVSS / PAni) bilayer films. An equivalent electrical circuit represented by $R_1(Q_1[R_2W_1])(Q_2[R_3(Q_3[R_4(Q_4[R_5W_2])])])$, in Boukamp's notation [29] (full line), was used to simulate the experimental results.

Table 6
Summary of the parameters associated to the uncovered, 08 and 10 self-assembled bilayer films covering the AA2024 alloy surfaces and corrosion reactions occurring in the respective surfaces. The parameters were obtained by fitting the EIS results with the proposed equivalent electrical circuit models.

Parameter	Bare AA2024 alloy	08 self-assembled bilayer films	10 self-assembled bilayer films
C_{Film} or Q_{film} (μF)	–	9.4	37.4
R_{Film} (Ω)	–	244	22.8
R_{ct} (kΩ)	11.0	54.3	16.3

Table 7
Inhibiting efficiency (η) of the multilayer films formed on the AA2024 alloy surfaces exposed to 0.1 mol L^{-1} NaCl aqueous solution.

Number of multilayers	Inhibiting efficiency (η) %
8 bilayers	80.0
10 bilayers	33.0

surface coated with film 10 (PVSS / PAni) bilayer films and exposed to the 0.1 mol L^{-1} NaCl aqueous solution. The fitting simulation was performed with the equivalent electrical circuit model shown in Fig. 8.

A comparison between the experimental results and the simulation performed with the equivalent electrical circuit shown in Fig. 8 (full line), indicates that the proposed model is adequate to explain the behavior of the AA2024 alloy surface coated with 10 (PVSS / PAni) bilayer films and exposed to the NaCl aqueous solution. Table 5 shows the parameter values obtained by the simulation of the EIS data using the proposed equivalent electric circuit.

Table 6 summarizes the EIS parameters associated to the films and corrosion reactions, i.e., capacitance and resistance of the films and resistance of the corrosion reactions (R_{ct}), obtained from fitting the experimental impedance data using the respective proposed models.

Comparing the values of Table 6, the capacitance of the 10 bilayers (PVSS / PAni) bilayer films covering the AA2024 alloy surfaces is bigger than that of the 08 bilayer films. As the thickness of the 10 bilayers should be bigger than that one of the 08 bilayer films covering the AA2024 alloy surfaces, and presuming that the area of the films coating the surfaces exposed to the chloride containing solution is the same, the bigger capacitance of the of the 10 bilayer films would be explained if the dielectric constant of these films was bigger than the one of the 08 bilayer films, due to, for instance, a bigger electrolyte solution diffusion into those first films. This explanation also justifies the smaller values of the corrosion reaction resistance (R_{ct}) observed for AA2024 alloy surfaces coated with 10 (PVSS / PAni) bilayer films in relation to those of surfaces coated with 08 (PVSS / PAni) bilayer films. These results also reinforce the previous pontiodynamic polarization and chronoamperometric results, that is, 08 is the optimum number of (PVSS / PAni) bilayers to better protect AA2024 alloy surface exposed to chloride containing media against corrosion.

From the EIS results shown in Table 6, the inhibiting efficiency (η) of the films covering the AA2024 alloy surface was calculated using Eq. (2), where R_{ct} is the resistance to charge transfer of corrosion reactions, values shown in Table 6. Table 7 shows the results of these calculations.

$$\eta = 1 - \frac{(Rct_{without/film})}{(Rct_{with/film})} \times 100 \quad (2)$$

The values of the inhibiting efficiency (η) obtained from the electrochemical impedance spectroscopy results (Table 7) are compatible with those obtained, respectively, from the chronoamperometric and potentiodynamic polarization results.

Fig. 10 shows the SEM micrographs of AA2024 alloy coated with film PVSS and (PVSS / PAni) multilayer films.

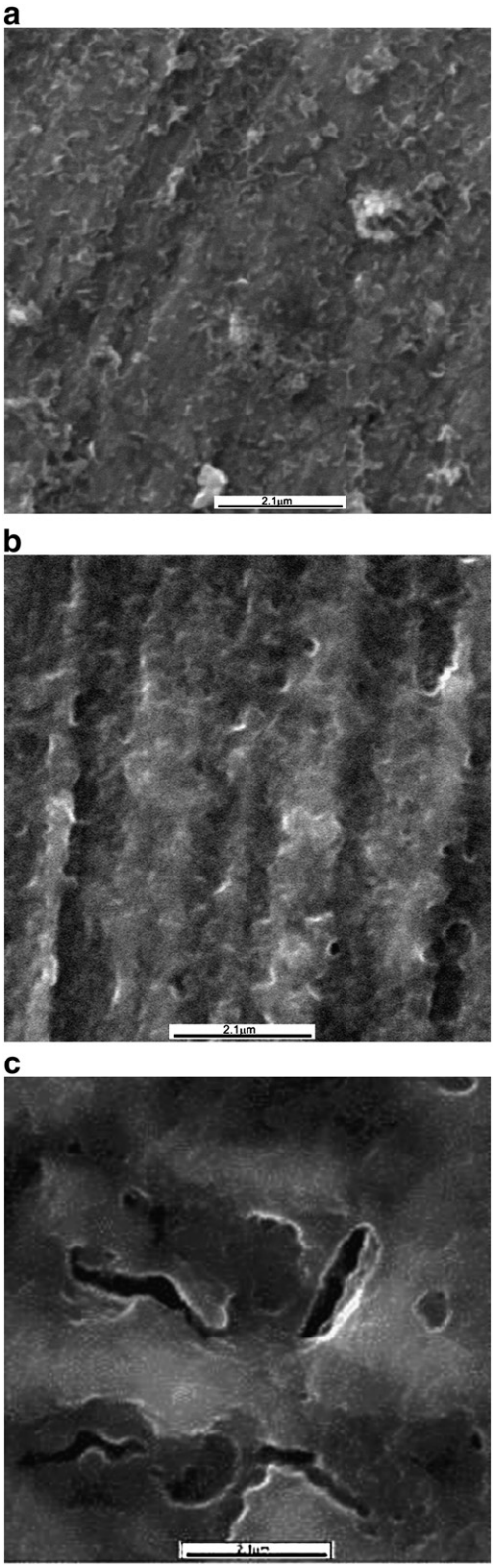

Fig. 10. SEM micrographs for AA2024 alloy surface coated with: (a) 01 PVSS layer (b) 08 and (c) 10 (PVSS / PAni) bilayer films.

The SEM micrograph in Fig. 10a shows that a non-homogeneous 01 PVSS layer film is formed on the aluminum alloy surface when they are immersed in the PVSS solution. By alternating the immersion in the PVSS aqueous solution and in the PAni-HCOOH formic acid aqueous solution, the negatively charged film of PVSS formed on the aluminum alloy surface eletctrostaticaly interacts with the positively

Table 8
Comparison of the EIS results obtained in this work, in chloride containing aqueous solution, for the AA2024 alloy surfaces coated with 08 (PVSS / PAni) bilayer films with those published for the system $(PPV|PSS)_3$ [35].

Parameter	This work	Reference [35]
	$(PVSS / PAni)_8$	$(PSS|PPV)_3$
C_f ($\mu F\ cm^{-2}$)	9.43	6.2
R_f ($\Omega\ cm^2$)	244	115
R_{ct} ($k\Omega\ cm^2$)	54.3	0.170

charged doped-PAni in solution forming a multilayer film of (PVSS / PAni), which composition was confirmed by FTIR results (not showed in this work, but that will be presented elsewhere). The SEM micrograph in Fig. 10b shows that the 08 layer-by-layer grown (PVSS / PAni) films formed on AA2024 alloy surfaces present pinholes and are very rough, while Fig. 10c shows that the 10 (PVSS / PAni) films are more homogeneous than the 08 (PVSS / PAni) bilayer films. However, the 10 (PVSS / PAni) bilayer films covering the aluminum alloy surface present big cracks that should be responsible for their worst performance on protecting the aluminum alloy surface against corrosion in NaCl containing media.

Table 8 presents a comparison of the EIS data (film capacitance (C_f), film resistance (R_f) and charge transfer resistance (R_{ct})) of the AA2024 alloy surfaces coated with 08 (PVSS / PAni) bilayer films, deposited in this work using the layer-by-layer growth technique, and some EIS results for surfaces coated with similar systems. At this point, it is worthwhile to point out that the closest to the systems studied in this work found in literature were the self-assembled films of the conducting polymer poly(*p*-phenylene vinylene) (PPV), and the polyanion poly(sodium 4-styrenesulfonate) (PSS) [35]. In this last case the self-assembled films were deposited on cysteamine hydrochloride (cyst) modified surfaces of gold-coated glasses to produce a three (PSS/PPV) bilayer film—$(PPV|PSS)_3$.

The film capacitance (C_f), film resistance (R_f) and charge transfer resistance (R_{ct}) of the AA2024 alloy surfaces coated with 08 (PVSS / PAni) bilayer—$(PVSS/PAni)_8$—film and those of the $(PPV|PSS)_3$ system have the same magnitude value. The differences between each of these EIS parameters can be attributed mainly to differences in the multilayer film constitution and the composition of the electrolyte in the electrochemical cell used to perform the EIS experiments: 0.1 M NaCl aqueous solution in this work and 5 mM $K_3[Fe(CN)_6]$ and $K_4[Fe(CN)_6]$ (1:1) in 0.025 M sodium phosphate solution in the EIS studies of the $(PPV|PSS)_3$ system. Therefore, the equivalent electrical circuits proposed to fit the EIS results in this work are adequate to explain the studied systems.

The next step for continuing this research is the synthesis of polyaniline used as dopant poly (acid vinylsulfonic salt sodium), and later, the synthesis will be made to characterize the new material PAni-PVSS, which application is the deposition of metals and preparation of catalysts with application in different materials.

4. Conclusions

The potentiodynamic polarization tests for the AA2024 alloy surface coated with different numbers of layer-by-layer deposited (PVSS / PAni) bilayers showed that, independent on the number of bilayers, the corrosion potential (Ecorr) of the aluminum alloy coated surface shifted to less negative values. This displacement is bigger for surfaces coated with a number of 08 bilayers, indicating that the surface has a smaller tendency to corrode. The corrosion current density (Jcorr) is also lower for the surface coated with 08 bilayers of (PVSS / PAni). Therefore, 08 is the number of (PVSS / PAni) bilayers that offers better corrosion protection to the AA2024 alloy surface in the environment containing chloride.

The inhibiting efficiency (η) afforded by the different numbers of (PVSS / PAni) bilayers deposited layer-by-layer was also determined by potentiodynamic polarization (93%), chronoamperometry (70%) and EIS (80%). The inhibiting efficiency (η) determined by these three different methods showed the same trend, i.e., 08 is the number of (PVSS / PAni) bilayers offering better corrosion protection to the AA2024 alloy surface in the environment containing chloride.

SEM micrographs of AA2024 alloy surfaces coated with 08 (PVSS / PAni) bilayers showed that these films present pinholes and are very rough, while the 10 bilayer films are more homogeneous. However, the last films present big cracks that facilitate diffusion of the NaCl containing electrolyte solution through the film. The morphology of these two films would explain not only the potentiodynamic polarization and chronoamperometric results but also the EIS results that indicate that 08 is the optimum number of PVSS / PAni bilayers to better protect AA2024 alloy surfaces exposed to chloride containing media against corrosion.

Acknowledgements

The authors thank the Instituto Tecnológico de Aeronáutica (ITA), the Conselho Nacional de Desenvolvimento Científico e Tecnológico (CNPq), and the Instituto Nacional de Pesquisas Espaciais (INPE) for, respectively, the financial support and help with the scanning electron microscopy (SEM) analyses.

References

[1] M.M. Attar, J.D. Scantlebury, J. Corros. Sci. Eng. 1 (1997) 1.
[2] N.M. Martyak, P. McAndrew, Corros. Sci. 49 (2007) 3826.
[3] A. Cook, A. Gabriel, N. Laycock, J. Electrochem. Soc. 151 (2004) 529.
[4] A. Gabriel, N. Laycock, H.N. Murray, G. Willians, A. Cook, Electrochem. Solid State Lett. 9 (2006) 57.
[5] S. Shreepathi, H.V. Hoang, R. Holze, J. Electrochem. Soc. 154 (2007) C67.
[6] N.A. Ogurtsov, A.A. Pud, P. Kamarchik, G.S. Shapoval, Synth. Met. 143 (2004) 43.
[7] D. Huerta-Vilca, S.R. Moraes, A.J. Motheo, Synth. Met. 140 (2004) 23.
[8] L. Zhong, S. Xiao, J. Hu, H. Zhu, F. Gan, Corros. Sci. 48 (2006) 3960.
[9] K. Rajendraprasad, N. Munichandraiah, J. Electrochem. Soc. 149 (2002) 1393.
[10] K.S. Ananda, M.K. Shree, T.S.N. Sankaranarayanan, S. Srikanth, Prog. Org. Coat. 62 (2008) 285.
[11] E.M. Geniès, A. Boyle, M. Lapkowski, Synth. Met. 36 (1990) 139.
[12] D.C. Trivedi, H.S. Nalwa (Eds.), Handbook of Organic Conductive Molecules and Polymers, vol. 2, Wiley, New York, 1997, p. 505.
[13] N.J. Pinto, C.M. Torres, P.K. Kahol, B.J. McCormick, J. Appl. Phys. 79 (1996) 8512.
[14] D.E. Tallman, Y. Pae, G.P. Bierwagen, Corrosion 56 (2000) 401.
[15] D.E. Tallman, G. Spinks, A. Dominis, G.G. Wallace, J. Solid State Electrochem. 6 (2002) 73.
[16] K. Shah, J. Iroh, Synth. Met. 132 (2002) 35.
[17] J. Stejskal, R.G. Gilbert, Pure Appl. Chem. 74 (2002) 857.
[18] J. Stejskal, P. Kratochvil, A.D. Jenkins, Collect. Czech. Chem. Commun. 60 (1995) 1747.
[19] A.C. Fou, M.F. Rubner, Macromolecules 28 (1995) 7115.
[20] J.H. Cheung, W.B. Stockton, M.F. Rubner, Macromolecules 30 (1997) 2712.
[21] A.G. MacDiarmid, J.C. Chiang, W.S. Huang, B.D. Humphery, N.L.D. Somasiri, Mol. Cryst. Liq. Cryst. 125 (1985) 309.
[22] A. Dan, P.K. Sengupta, J. Appl. Pol. Sci. 91 (2004) 991.
[23] L. Sun, S.C. Yang, J.-M. Liu, Mater. Res. Soc. Symp. Proc. 328 (1994) 209.
[24] A.C. Fou, O. Onitsuka, M. Ferreira, M.F. Rubner, B.R. Hsieh, J. Appl. Phys. 79 (1996) 7501.
[25] Installation and Diagnostics Guide for μAUTOLAB Type II (2001) Autolab with PGSTAT30 Eco Chemie B.V. P°. Box 85163, 305 AD Utrecht, Netherlands.
[26] W.J. Lorenz, F. Mansfeld, Corros. Sci. 21 (1981) 646.
[27] M. Tussolini, C. Spagnol, E.C. Gomes, M.T. Cunha, P.R.P. Rodrigues, Rev. Esc. Minas 60 (2007) 41.
[28] M.A.S. Oliveira, J.J. Moraes, R. Faez, Prog. Org. Coat. 65 (2009) 348.
[29] B.A. Boukamp, Solid State Ionics 20 (1986) 31.
[30] J. Bisquert, A. Compte, J. Electroanal. Chem. 499 (2001) 112.
[31] Z.H. Liu, J.F. Zhao, J. McLaughlin, Diamond Relat. Mater. 8 (1999) 56.
[32] J. Navarro-Laboulais, J.J. Garcia-Jareno, F. Vicente, J. Electroanal. Chem. 536 (2002) 11.
[33] Z. Kerner, T. Pajkossy, Electrochim. Acta 46 (2000) 207.
[34] T. Pajkossy, Solid State Ionics 176 (2005) 1997.
[35] R.N. Vyas, B. Wang, Int. J. Mol. Sci. 11 (2010) 1956.